International Journal of
Automotive Manufacturing and Materials (IJAMM)

Scilight

Article

Check for updates

Effects of Suspension Stiffness, Vehicle Speed, and Road Roughness on Dynamic Loading of the Drive Axle Housing in a 1.25-Ton Light Truck

Luong Van Van *, To Ngoc Luat †, Tran Thi Ngoc Truc †, Dang Hai Dang †, and Nguyen Thanh Dong †

Faculty of Mechanical and Automotive Engineering, Vinh Long University of Technology and Engineering (VLUTE), Vinh Long 85000, Vietnam

* Correspondence: vanlv@vlute.edu.vn

† These authors contributed equally to this work.

Received: 29 July 2026; Revised: 23 October 2026; Accepted: 5 November 2026; Published: 17 November 2026

Abstract: This paper investigates the effects of rear suspension stiffness on dynamic loading of the drive axle housing of a 1.25-ton light truck under random excitation, in accordance with ISO 8608:2016. A full-vehicle oscillation model was constructed to simulate dynamic loads over a speed range of 20–60 km/h for four road classes: B, C, D, and E. Two evaluation criteria were used: maximum dynamic load coefficient (K_{dmax}) and minimum dynamic load coefficient (K_{dmin}). The results show that road surface quality has a greater influence than speed and suspension stiffness. The traction reduction is high, while K_{dmax} increases from 1.05 to 2.02 (92.4%) when the road class changes from B to E at 60 km/h, and K_{dmin} decreases from 0.40 to 0.19 (52.5%). For road class E at 60 km/h, when the suspension stiffness increases from 0.5*C to 1.5*C, the K_{dmax} increases from 1.82 to 2.30 (26.4%), while the K_{dmin} decreases from 0.22 to 0.17 (22.7%). The worst case is for road class E with a stiffness of 1.5*C, where K_{dmax} = 2.30, corresponding to a dynamic load exceeding the static load by 130%, and K_{dmin} = 0.17, approaching the condition of loss of wheel contact with the road surface.

Keywords: drive axle housing; dynamic loading; Suspension stiffness; road roughness; ISO 8608 random road excitation

1. Introduction

The rapid development of road transportation has significantly increased the demand for light-duty trucks because of their flexibility, high operational efficiency, and relatively low transportation cost. In developing nations, especially in Vietnam, 1.25-ton light trucks are commonly used for urban logistics, agricultural transportation, and regional freight distribution [1]. Because of their high operating frequency and varying pavement conditions, these vehicles experience complex dynamic excitations from road-surface irregularities. The drive axle housing is a critical structural component that transmits vertical, longitudinal, and lateral loads while supporting the differential assembly and suspension system [2]. The axle housing is subjected to static loading and continuously varying dynamic loads throughout vehicle operation due to uneven road profiles, vehicle speed, suspension characteristics, and payload conditions [3].

Numerous studies have investigated vehicle vertical dynamics using quarter-car, half-car, and full-vehicle models. These models have been extensively applied to evaluate ride comfort, handling stability, tire dynamic loads, suspension performance, and vehicle safety under various road excitations. Faris et al. [4] compared the ride performance and dynamic characteristics of passive and semi-active suspension systems using different vehicle models. Munawwarah and Yakub [5] investigated vehicle ride comfort through integrated control strategies applied to quarter-car and half-car active suspension models.

Abramov et al. [6] investigated semi-active suspension performance through Simulink-based simulations, while Nhu et al. [7] developed a physics-guided reinforcement learning approach for active suspension control under realistic vehicle operating conditions. The combination of multi-degree-of-freedom dynamic models and ISO 8608 stochastic road excitation has therefore become the dominant approach in vehicle vibration research [8]. The 1.25-ton light truck investigated in this study is shown in Figure 1.

Copyright: © 2026 by the authors. This is an open access article under the terms and conditions of the Creative Commons Attribution (CC BY) license (https://creativecommons.org/licenses/by/4.0/).
Publisher's Note: Scilight stays neutral with regard to jurisdictional claims in published maps and institutional affiliations.



Figure 1. 1.25-ton light truck.

Figure 2 illustrates the vehicle vibration models considered in this study, including (a) the quarter-car suspension model and (b) the half-car suspension model.

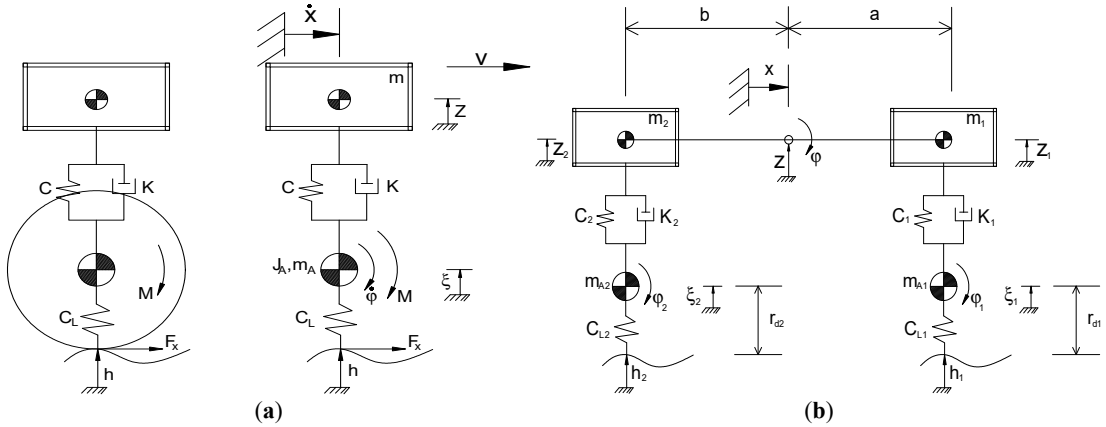


Figure 2. Vehicle vibration model. (**a**). Quarter-car suspension model; (**b**). Half-car suspension model.

Figure 3 illustrates the uneven road surface profiles corresponding to different road roughness classes according to ISO 8608.

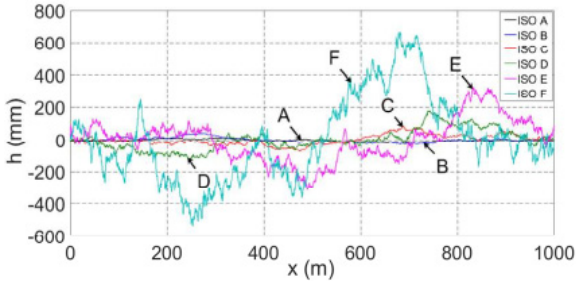


Figure 3. Uneven road surface ISO 8608.

A light vehicle drive axle housing is subject to complex loading conditions during operation [9]. In addition to static loads arising from the weight of the vehicle and its load, the axle housing is subjected to dynamic loads from road imperfections, suspension movement, tire deformation, accelerating, braking, and the power gearbox [10,11]. Among these factors, vertical dynamic loading due to road roughness is particularly important, as it is always present during normal driving and can significantly increase stress amplitude in critical structural regions [12].

Road roughness is one of the main external excitations responsible for vehicle vibration and dynamic load variation. In vehicle dynamics research, road surfaces are commonly modeled as random processes characterized by their power spectral density (PSD). ISO 8608 provides a widely used framework for describing and classifying

road surface roughness based on the spatial PSD of road profiles [13]. The interaction between road roughness and vehicle speed determines the excitation frequency content experienced by the suspension system, thereby affecting both vehicle vibration and dynamic wheel loads [14,15].

Hua et al. [16] investigated the random vibration characteristics of vehicles with hysteretic nonlinear suspensions under road roughness excitation. Misaghi et al. [17] examined the influence of pavement roughness and suspension systems on vehicle dynamic loads. Wei et al. [18] analyzed the nonlinear dynamic behavior and energy transfer of an automobile shimmy system considering road roughness excitation. The influence of suspension stiffness is particularly complex under random road excitation because its effect depends on the frequency distribution of road roughness. When the dominant excitation frequencies overlap with the suspension system's dynamic characteristics, changes in suspension stiffness can significantly alter the amplitude of the dynamic response. Therefore, the effect of suspension stiffness should be evaluated over a range of road roughness levels and vehicle speeds rather than under a single operating condition.

The damping coefficient determines the suspension system's ability to absorb vibration energy and regulate oscillations. Increasing damping can suppress resonance and reduce transient oscillations, especially around the suspension system's inherent frequency. However, excessive damping will degrade suspension isolation and increase the transmission of high-frequency road excitation into the vehicle body and structural components [18,19]. Zhang et al. [19] demonstrated that the energy dissipation characteristics of a suspension system are closely related to its dynamic response under random road excitation. Their results suggest that suspension damping should be selected by considering the interaction between ride comfort, energy dissipation, and road excitation characteristics rather than by maximizing damping alone. Nazemi et al. [20] investigated a series active variable-geometry suspension using a full-vehicle model and robust control to improve roll dynamics and tire–road contact under rough road conditions. Similarly, Najafi and Masih-Tehrani [21] examined vehicle roll stability using an active variable-geometry suspension and different control strategies. These studies highlight the importance of suspension characteristics and coupled vehicle dynamics in evaluating vehicle performance. However, the present study focuses specifically on vertical dynamic loading of the rear drive axle housing, while lateral load transfer and multi-axial structural loading remain outside its scope.

Although previous studies have extensively investigated vehicle suspension dynamics, ride comfort, and dynamic wheel loads, fewer studies have specifically examined the influence of suspension stiffness on the vertical dynamic loading of drive axle housings in light-duty trucks. Satyanarayana et al. [22] investigated the optimization of vehicle suspension parameters to improve ride comfort. Deremetz et al. [23] proposed real-time stiffness and damping control strategies for adjustable suspensions to reduce vehicle dynamic responses under off-road operating conditions, while Wang et al. [24] evaluated dynamic load coefficients using a multibody dynamics model of a six-axle heavy truck. However, the combined effects of suspension stiffness, vehicle speed, and ISO 8608 road roughness on the dynamic loading of a light-truck drive axle housing remain insufficiently characterized.

It should be emphasized that dynamic force refers to the time-varying external load acting on the axle housing, whereas dynamic stress represents the resulting internal structural response, which requires further structural analysis. Accordingly, the present study focuses on quantifying vertical dynamic forces and their maximum and minimum dynamic load coefficients (K_{dmax} and K_{dmin}), rather than directly evaluating structural stresses or fatigue damage. These results provide a basis for subsequent structural durability assessments.

Hamid Gheibollahi et al. [25] investigated vehicle suspension responses under non-stationary random road excitation using evolutionary spectral analysis, considering ride comfort and suspension energy dissipation. Their findings highlight the importance of evaluating multiple performance characteristics when investigating suspension dynamics. In contrast, the present study focuses on the effects of rear suspension stiffness, vehicle speed, and road roughness on vertical dynamic wheel loads, providing complementary information for subsequent axle housing durability assessments.

These limitations indicate a lack of an integrated understanding of the relationship between suspension parameters, random road excitation, vehicle speed, and dynamic axle housing loading. In particular, the combined effects of suspension stiffness, vehicle speed, and road roughness on the vertical dynamic loading of light-truck drive axle housings have not been sufficiently investigated under the operating conditions considered in this study. This gap is important because dynamic forces generated by road irregularities are transmitted through the tire–suspension system and ultimately contribute to the cyclic loading experienced by the axle housing. Previous failure investigations have also shown that dynamic forces associated with actual road conditions can contribute to fatigue damage and failure of drive axle housings, highlighting the importance of considering realistic dynamic loading conditions in axle durability assessment [10].

To address these gaps, the present study investigates the effects of suspension stiffness on the dynamic vertical loads acting on the drive axle housing of a 1.25-ton light truck under random road excitation. A full-

vehicle dynamic model is developed to evaluate the dynamic axle load under different ISO 8608 road roughness classes and vehicle speeds. The maximum dynamic axle load and dynamic load coefficient are employed as the primary indicators to quantify the sensitivity of axle loading to suspension parameters. The main contribution of this study is the quantitative evaluation of the effects of rear suspension stiffness, vehicle speed, and road roughness on vertical dynamic wheel loads. The results provide useful information on the loading conditions associated with the rear axle and serve as a basis for future structural strength and fatigue-life assessments of the drive axle housing.

Since the research subject is the dynamic load acting on the drive axle housing of a truck, the author chose two criteria for evaluation in this study: dynamic load and dynamic safety, which are defined as follows:

Dynamic load criteria: This is evaluated through the value of the maximum dynamic load coefficient K_{dmax} at the wheels [1,2,26,27].

$$K_{d\max} = 1 + \frac{\max(F_{CLij})}{F_{Gij}} \leq 2{,}5$$

where:

F_{CLij}: reaction force of the tire;
F_{Gij}: Static load at the wheel.

The criterion $K_{dmax} \leq 2.5$ is adopted from previous studies as a reference limit for evaluating the magnitude of dynamic wheel loading. A value of $K_{dmax} = 2.5$ indicates that the maximum vertical wheel load reaches 2.5 times the corresponding static load. This threshold is used as an engineering evaluation criterion for dynamic loading rather than a directly established structural safety factor or fatigue limit of the axle housing.

Dynamic safety criteria: Evaluated through the minimum dynamic loading coefficient K_{dmin}, which allows assessment of the reduction in wheel power transmission capacity, determined as follows ([1,2,26,27]):

$$K_{d\min} = 1 + \frac{\min(F_{CLij})}{F_{Gij}}$$

$K_{dmin} = 0.5$: warning limit;
$K_{dmin} = 0$: limited intervention.

The present study focuses on the effects of rear suspension stiffness, vehicle speed, and road roughness, while the damping coefficients are maintained constant throughout the simulations. The remainder of this paper is organized as follows. Section 2 presents the full-vehicle dynamic model and its governing equations. Section 3 investigates the dynamic loads acting on the drive axle housing under different road roughness conditions and vehicle speeds. Section 4 examines the influence of rear suspension stiffness on dynamic load characteristics. Section 5 presents the experimental validation of the vehicle dynamic model. Finally, Section 6 summarizes the main findings, limitations, and directions for future research.

For each road roughness class and vehicle speed, the vertical dynamic wheel force was obtained from the simulated time history. The instantaneous dynamic load coefficient was calculated as the ratio of the vertical wheel force to the corresponding static wheel load. The maximum and minimum dynamic load coefficients were then determined from the highest and lowest values of this ratio over the simulation interval, respectively. Accordingly, each data point represents the extreme value extracted from the corresponding stochastic force time history rather than an average value. This procedure was applied consistently to all investigated road conditions and vehicle speeds.

2. Vehicle Dynamic Model

Trucks have complex structures with nonlinear geometric and physical linkages, significantly affecting their dynamic properties, especially under critical motion conditions. Therefore, nonlinearity is essential in current dynamic research. Truck structures are characterized by a load-bearing frame, a dependent suspension system with high physical nonlinearity, and a body divided into front and rear suspension sections, each corresponding to a front or rear axle. Given these structural characteristics, this study makes the following assumptions to describe the dynamics of a 2-axle truck:

(1) The 1.25-ton light truck model has two symmetrical axles along the vehicle's longitudinal axis.

(2) The vehicle body is considered a flat plate with mass m_s located at the center of gravity, with 3 movements including: translational movement along the vertical axis z_s and 2 corresponding rotation angles: θ_{sy} (longitudinal oscillation angle—rotation around the horizontal axis y), θ_{sx} (lateral oscillation angle—rotation around the longitudinal axis x).

(3) The axles have masses m_{u1} and m_{u2} located at their centers of gravity. Each axle has a translational motion along the vertical axis (Z_{u1}, Z_{u2}) and an angular displacement around the longitudinal axis (θ_{u1}, θ_{u2}).

(4) The vehicle body is connected to the axles via a suspension system (characterized by stiffness C and damping coefficient K).

(5) In the vertical plane, number 1 represents the front axle; number 2 represents the rear axle; in the horizontal plane, number 1 represents the left side, number 2 represents the right side.

(6) The vehicle's axle is connected to the road surface by elastic wheels, characterized by stiffness values C_L and damping coefficients K_L.

(7) Aerodynamic forces are neglected in the present model because the investigated vehicle speed is limited to 60 km/h. Within this speed range, aerodynamic effects are assumed to have a relatively minor influence on the vertical dynamic response compared with road-induced excitation.

(8) Tire-road contact is assumed to be point contact with the road surface.

With such structural assumptions, the truck's dynamic model can be described as shown above (Figure 4).

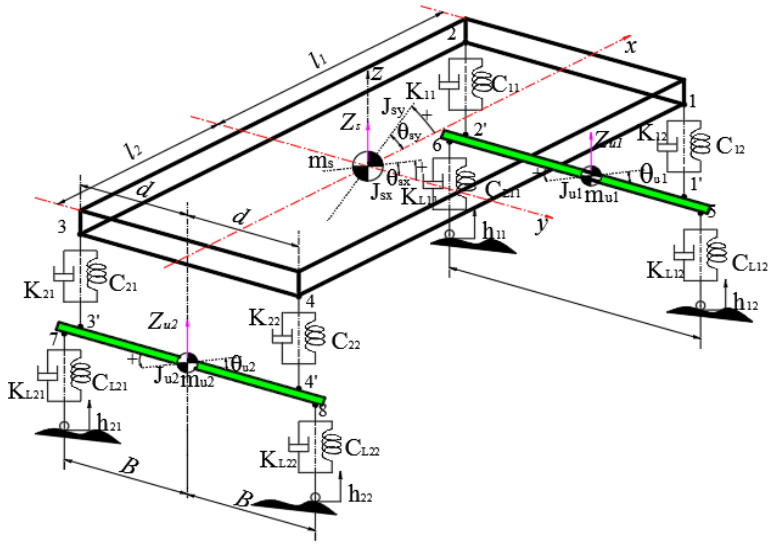


Figure 4. Dynamic model of a two-axle truck in space.

Figure 4 describes the three-dimensional dynamic model of the two-axle truck. The seven degrees of freedom (DOFs) are defined as follows: Z_s is the vertical displacement of the sprung mass; θ_{sx} and θ_{sy} are the roll and pitch angles of the sprung mass, respectively; Z_{u1} and Z_{u2} are the vertical displacements of the front and rear unsprung masses, respectively; and θ_{u1} and θ_{u2} are the corresponding roll angles of the front and rear unsprung masses.

Figure 5 describes the dynamic model of the two-axle truck in the longitudinal vertical plane Oxz. The relevant DOFs are Z_s, θ_{sy}, Z_{u1}, and Z_{u2}, as defined in Figure 4.

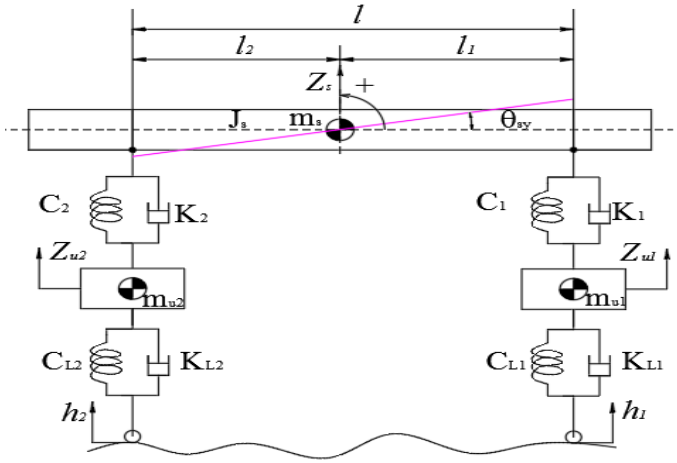


Figure 5. Dynamic model of a two-axle truck in the longitudinal vertical plane Oxz.

Figure 6 describes the dynamic model of the two-axle truck in the transverse plane Oyz. The relevant DOFs are Z_s, θ_{sx}, Z_{u1}, Z_{u2}, θ_{u1}, and θ_{u2}, as defined in Figure 4.

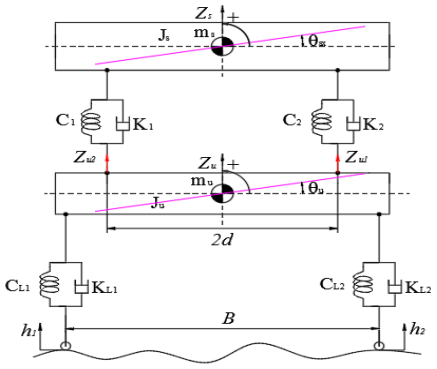


Figure 6. Dynamic model of a two-axle truck in the transverse vertical plane Oyz.

Where:

+ Z_s—Displacement of the sprung mass in the Z-axis.
+ Z_{u1}, Z_{u2}—The displacement of the unsprung mass from the front and rear axles in the Z-axis.
+ m_s—Sprung mass.
+ m_{u1}, m_{u2}—Unsprung mass from the front axle and rear axle.
+ J_{sx}, J_{xy}—Moment of inertia of a sprung mass rotating around the X-axis and Y-axis.
+ J_{u1}, J_{u2}—Moment of inertia of an unsprung mass from the front and rear axle.
+ θ_{sy}, θ_{sx}—The angle of rotation of the sprung mass around the Y-axis and X-axis.
+ θ_{u1}, θ_{u2}—The angle of rotation of the unsprung mass around the X-axis at the front and rear axles.
+ C_{11}, C_{12}, C_{21}, C_{22}—Stiffness of the front left, front right, rear left, and rear right suspension systems.
+ K_{11}, K_{12}, K_{21}, K_{22}—Damping coefficients of the front left, front right, rear left, and rear right suspension systems.
+ C_{L11}, C_{L12}, C_{L21}, C_{L22}—Tire stiffness of the front left, front right, rear left, and rear right.
+ K_{L11}, K_{L12}, K_{L21}, K_{L22}—Front left, front right, rear left, and rear right tire damping coefficients.
+ B—The distance from the vehicle's center to the center of the left or right wheel.
+ *d*—The distance from the vehicle's center to the left or right suspension linkage point.
+ l_1, l_2—The distance from the vehicle's center to the center of the front and rear axles.
+ h_{11}, h_{12}, h_{21}, h_{22}—Road surface unevenness height at front left, front right, rear left, and rear right wheels.

The main parameters of the investigated 1.25-ton light truck, including mass properties, suspension stiffness and damping coefficients, tire characteristics, and geometric dimensions, are summarized in Table 1. These parameters were adopted from a previous master's thesis [28] and used as input data for the full-vehicle dynamic model.

Table 1. Parameters of the 1.25-ton light truck dynamic model.

Parameter	Symbol	Value	Unit
Sprung mass	m_s	2800	kg
Front axle unsprung mass	m_{u1}	300	kg
Rear axle unsprung mass	m_{u2}	400	kg
Sprung mass moment of inertia about the x-axis	J_{sx}	4403	kg·m^2
Sprung mass moment of inertia about the y-axis	J_{sy}	16,645	kg·m^2
Front axle moment of inertia	J_{u1}	285	kg·m^2
Rear axle moment of inertia	J_{u2}	335	kg·m^2
Front-left suspension stiffness	C_{11}	175,000	N/m
Front-right suspension stiffness	C_{12}	175,000	N/m
Rear-left suspension stiffness	C_{21}	326,000	N/m
Rear-right suspension stiffness	C_{22}	326,000	N/m
Front-left suspension damping coefficient	K_{11}	6090	N·s/m
Front-right suspension damping coefficient	K_{12}	6090	N·s/m
Rear-left suspension damping coefficient	K_{21}	7675	N·s/m
Rear-right suspension damping coefficient	K_{22}	7675	N·s/m
Front tire stiffness (left/right)	C_{L11}, C_{L12}	350,000	N/m
Rear tire stiffness (left/right)	C_{L21}, C_{L22}	652,000	N/m
Front tire damping coefficient (left/right)	K_{L11}, K_{L12}	7985	N·s/m
Rear tire damping coefficient (left/right)	K_{L21}, K_{L22}	8640	N·s/m
Suspension attachment half-spacing	*d*	1050	mm
Wheel-track parameter	B	1400	mm
Wheelbase	$l = l_1 + l_2$	2670	mm

Apply the Newton-Euler equation to the three oscillating masses:

(1) The sprung mass consists of: Vertical motion along the Z-axis (Z_s), rotational motion around the X-axis (θ_{sx}), and rotational motion around the Y-axis (θ_{sy}).

(2) The unsprung mass from the front axle includes vertical motion along the Z-axis (Z_{u1}) and rotational motion around the X-axis (θ_{u1}).

(3) The unsprung mass from the rear axle includes vertical motion along the Z-axis (Z_{u2}) and rotational motion around the X-axis (θ_{u2}).

$$\begin{aligned}
&m_s\ddot{Z}_s = -K_{12}\left(\dot{Z}_s + \dot{\theta}_{sy}l_1 + \dot{\theta}_{sx}d - \dot{Z}_{u1} - \dot{\theta}_{u1}d\right) - C_{12}\left(Z_s + \theta_{sy}l_1 + \theta_{sx}d - Z_{u1} - \theta_{u1}d\right)\\
&-K_{11}\left(\dot{Z}_s + \dot{\theta}_{sy}l_1 - \dot{\theta}_{sx}d - \dot{Z}_{u1} + \dot{\theta}_{u1}d\right) - C_{11}\left(Z_s + \theta_{sy}l_1 - \theta_{sx}d - Z_{u1} + \theta_{u1}d\right)\\
&-K_{21}\left(\dot{Z}_s - \dot{\theta}_{sy}l_2 - \dot{\theta}_{sx}d - \dot{Z}_{u2} + \dot{\theta}_{u2}d\right) - C_{21}\left(Z_s - \theta_{sy}l_2 - \theta_{sx}d - Z_{u2} + \theta_{u2}d\right)\\
&-K_{22}\left(\dot{Z}_s - \dot{\theta}_{sy}l_2 + \dot{\theta}_{sx}d - \dot{Z}_{u2} - \dot{\theta}_{u2}d\right) - C_{22}\left(Z_s - \theta_{sy}l_2 + \theta_{sx}d - Z_{u2} - \theta_{u2}d\right)
\end{aligned} \tag{1}$$

$$\begin{aligned}
&J_{sy}\ddot{\theta}_{sy} = -K_{12}l_1\left(\dot{Z}_s + \dot{\theta}_{sy}l_1 + \dot{\theta}_{sx}d - \dot{Z}_{u1} - \dot{\theta}_{u1}d\right) - C_{12}l_1\left(Z_s + \theta_{sy}l_1 + \theta_{sx}d - Z_{u1} - \theta_{u1}d\right)\\
&-K_{11}l_1\left(\dot{Z}_s + \dot{\theta}_{sy}l_1 - \dot{\theta}_{sx}d - \dot{Z}_{u1} + \dot{\theta}_{u1}d\right) - C_{11}l_1\left(Z_s + \theta_{sy}l_1 - \theta_{sx}d - Z_{u1} + \theta_{u1}d\right)\\
&+K_{21}l_2\left(\dot{Z}_s - \dot{\theta}_{sy}l_2 - \dot{\theta}_{sx}d - \dot{Z}_{u2} + \dot{\theta}_{u1}d\right) + C_{21}l_2\left(Z_s - \theta_{sy}l_2 - \theta_{sx}d - Z_{u2} + \theta_{u1}d\right)\\
&+K_{22}l_2\left(\dot{Z}_s - \dot{\theta}_{sy}l_2 + \dot{\theta}_{sx}d - \dot{Z}_{u2} - \dot{\theta}_{u1}d\right) + C_{22}l_2\left(Z_s - \theta_{sy}l_2 + \theta_{sx}d - Z_{u2} - \theta_{u1}d\right)
\end{aligned} \tag{2}$$

$$\begin{aligned}
&J_{sx}\ddot{\theta}_{sx} = -K_{12}d\left(\dot{Z}_s + \dot{\theta}_{sy}l_1 + \dot{\theta}_{sx}d - \dot{Z}_{u1} - \dot{\theta}_{u1}d\right) - C_{12}d\left(Z_s + \theta_{sy}l_1 + \theta_{sx}d - Z_{u1} - \theta_{u1}d\right)\\
&+K_{11}d\left(\dot{Z}_s + \dot{\theta}_{sy}l_1 - \dot{\theta}_{sx}d - \dot{Z}_{u1} + \dot{\theta}_{u1}d\right) + C_{11}d\left(Z_s + \theta_{sy}l_1 - \theta_{sx}d - Z_{u1} + \theta_{u1}d\right)\\
&-K_{21}d\left(\dot{Z}_s - \dot{\theta}_{sy}l_2 + \dot{\theta}_{sx}d - \dot{Z}_{u2} - \dot{\theta}_{u2}d\right) - C_{21}d\left(Z_s - \theta_{sy}l_2 + \theta_{sx}d - Z_{u2} - \theta_{u2}d\right)\\
&+K_{22}d\left(\dot{Z}_s - \dot{\theta}_{sy}l_2 - \dot{\theta}_{sx}d - \dot{Z}_{u2} + \dot{\theta}_{u2}d\right) + C_{22}d\left(Z_s - \theta_{sy}l_2 - \theta_{sx}d - Z_{u2} + \theta_{u2}d\right)
\end{aligned} \tag{3}$$

$$\begin{aligned}
&m_{u1}\ddot{Z}_{u1} = -K_{12}\left(\dot{Z}_{u1} + \dot{\theta}_{u1}d - \dot{Z}_s - \dot{\theta}_{sy}l_1 - \dot{\theta}_{sx}d\right) - C_{12}\left(Z_{u1} + \theta_{u1}d - Z_s - \theta_{sy}l_1 - \theta_{sx}d\right)\\
&-K_{11}\left(\dot{Z}_{u1} - \dot{\theta}_{u1}d - \dot{Z}_s - \dot{\theta}_{sy}l_1 + \dot{\theta}_{sx}d\right) - C_{11}\left(Z_{u1} - \theta_{u1}d - Z_s - \theta_{sy}l_1 + \theta_{sx}d\right)\\
&-K_{L12}\left(\dot{Z}_{u1} + \dot{\theta}_{u1}B - \dot{h}_{12}\right) - C_{L12}\left(Z_{u1} + \theta_{u1}B - h_{12}\right)\\
&-K_{L11}\left(\dot{Z}_{u1} - \dot{\theta}_{u1}B - \dot{h}_{11}\right) - C_{L11}\left(Z_{u1} - \theta_{u1}B - h_{11}\right)
\end{aligned} \tag{4}$$

$$\begin{aligned}
&J_{u1}\ddot{\theta}_{u1} = -K_{12}d\left(\dot{Z}_{u1} + \dot{\theta}_{u1}d - \dot{Z}_s - \dot{\theta}_{sy}l_1 - \dot{\theta}_{sx}d\right) - C_{12}d\left(Z_{u1} + \theta_{u1}d - Z_s - \theta_{sy}l_1 - \theta_{sx}d\right)\\
&+K_{11}d\left(\dot{Z}_{u1} - \dot{\theta}_{u1}d - \dot{Z}_s - \dot{\theta}_{sy}l_1 + \dot{\theta}_{sx}d\right) + C_{11}d\left(Z_{u1} - \theta_{u1}d - Z_s - \theta_{sy}l_1 + \theta_{sx}d\right)\\
&-K_{L12}B\left(\dot{Z}_{u1} + \dot{\theta}_{u1}B - \dot{h}_{12}\right) - C_{L12}B\left(Z_{u1} + \theta_{u1}B - h_{12}\right)\\
&+K_{L11}B\left(\dot{Z}_{u1} - \dot{\theta}_{u1}B - \dot{h}_{11}\right) + C_{L11}B\left(Z_{u1} - \theta_{u1}B - h_{11}\right)
\end{aligned} \tag{5}$$

$$\begin{aligned}
&m_{u2}\ddot{Z}_{u2} = -K_{21}\left(\dot{Z}_{u2} - \dot{\theta}_{u2}d - \dot{Z}_s + \dot{\theta}_{sy}l_2 + \dot{\theta}_{sx}d\right) - C_{21}\left(Z_{u2} - \theta_{u2}d - Z_s + \theta_{sy}l_2 + \theta_{sx}d\right)\\
&-K_{22}\left(\dot{Z}_{u2} + \dot{\theta}_{u2}d - \dot{Z}_s + \dot{\theta}_{sy}l_2 - \dot{\theta}_{sx}d\right) - C_{22}\left(Z_{u2} + \theta_{u2}d - Z_s + \theta_{sy}l_2 - \theta_{sx}d\right)\\
&-K_{L21}\left(\dot{Z}_{u2} + \dot{\theta}_{u2}B - \dot{h}_{21}\right) - C_{L21}\left(Z_{u2} + \theta_{u2}B - h_{21}\right)\\
&-K_{L22}\left(\dot{Z}_{u2} - \dot{\theta}_{u2}B - \dot{h}_{22}\right) - C_{L22}\left(Z_{u2} - \theta_{u2}B - h_{22}\right)
\end{aligned} \tag{6}$$

$$
\begin{aligned}
J_{u2}\ddot{\theta}_{u2} = &-K_{21}d\left(\dot{Z}_{u2}-\dot{\theta}_{u2}d-\dot{Z}_s+\dot{\theta}_{sy}l_2+\dot{\theta}_{sx}d\right)-C_{21}d\left(Z_{u2}-\theta_{u2}d-Z_s+\theta_{sy}l_2+\theta_{sx}d\right)\\
&+K_{22}d\left(\dot{Z}_{u2}+\dot{\theta}_{u2}d-\dot{Z}_s+\dot{\theta}_{sy}l_2-\dot{\theta}_{sx}d\right)+C_{22}\left(Z_{u2}+\theta_{u2}d-Z_s+\theta_{sy}l_2-\theta_{sx}d\right)\\
&-K_{L21}B\left(\dot{Z}_{u2}+\dot{\theta}_{u2}B-\dot{h}_{21}\right)-C_{L21}B\left(Z_{u2}+\theta_{u2}B-h_{21}\right)\\
&+K_{L22}B\left(\dot{Z}_{u2}-\dot{\theta}_{u2}B-\dot{h}_{22}\right)+C_{L22}B\left(Z_{u2}-\theta_{u2}B-h_{22}\right)
\end{aligned}
\tag{7}
$$

3. Survey to Determine Dynamic Loads Acting on the Axle Housing

Four types of roads, according to ISO 8608:2016, were tested in this study, including: Type B (good road), Type C (average road), Type D (poor road), and Type E (very poor road). Road surface imperfections were uniformly distributed along two wheel tracks, with vehicles driving in a straight line. This was the case for the study under consideration, in which no lateral forces were applied, and the vehicle speeds ranged from 20 to 60 km/h.

The analysis results are the vertical force components (F_{z2}) applied to the axle housing. Additionally, this study evaluates dynamic load and safety criteria for road types B, C, D, and E.

The simulation results over time (Figures 7–10) show a distinct variation in the reaction force F_{z2}, strongly dependent on road surface quality and vehicle speed. On road classes B and C, K_{dmin} ranges from 0.32 to 0.48, remaining below the defined warning threshold of 0.50. Although these values are higher than those observed on rougher road classes D and E, they indicate a reduction in tire–road contact force and suggest potential concerns regarding vehicle dynamic safety rather than guaranteeing stable operation. On road types D and E (poor & very poor roads), the vertical force acting on the axle housing exhibits a very large variation amplitude. In particular, on road class E at 60 km/h, the maximum force applied reaches 2.02 times the static load, resulting in continuous mechanical impact on the axle housing.

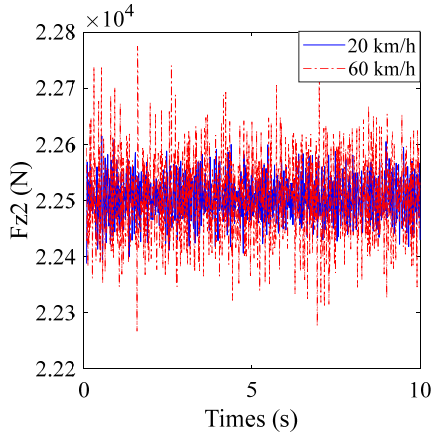


Figure 7. Time history of rear axle load F_{z2} on an ISO 8608 class B road.

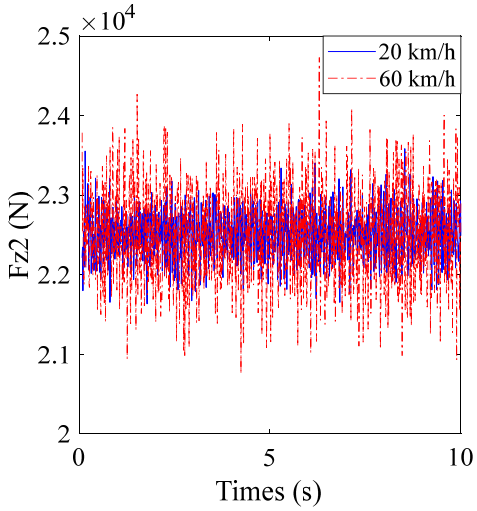


Figure 8. Time history of rear axle load F_{z2} on an ISO 8608 class C road.

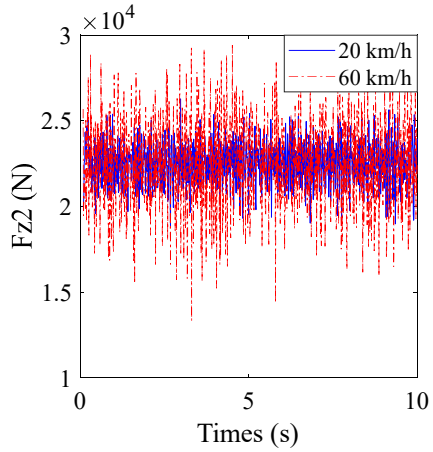


Figure 9. Time history of rear axle load F_{z2} on an ISO 8608 class D road.

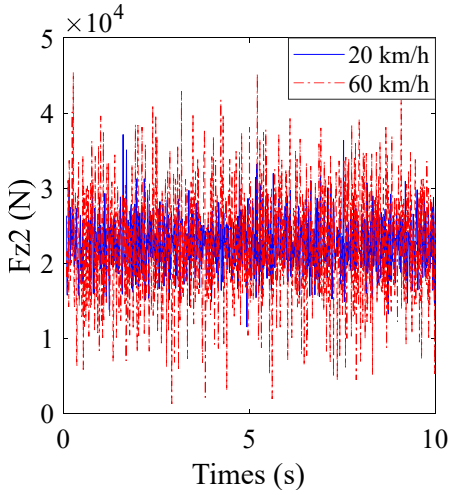


Figure 10. Time history of rear axle load F_{z2} on an ISO 8608 class E road.

Figure 11 illustrates the variation in the maximum dynamic load coefficient (K_{dmax}) with vehicle speed under different ISO 8608 road roughness classes. The results show that K_{dmax} generally increases with vehicle speed and road roughness, with the highest values observed on road class E. Figure 12 presents the variation in the minimum dynamic load coefficient (K_{dmin}) with vehicle speed under different road roughness classes. K_{dmin} decreases as vehicle speed and road roughness increase, indicating a progressive reduction in the minimum tire–road contact force. The corresponding numerical results of K_{dmax} and K_{dmin} under different vehicle speeds and ISO 8608 road roughness classes are summarized in Table 2.

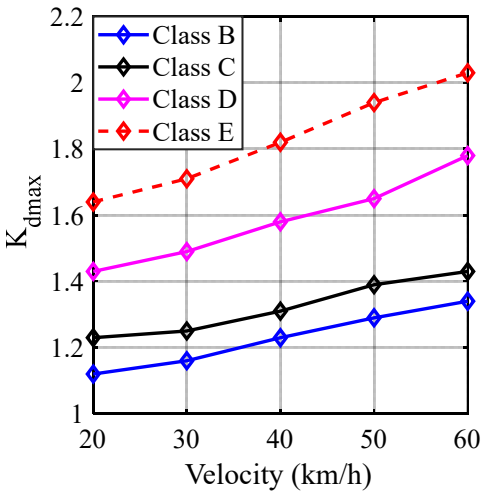


Figure 11. K_{dmax} varies across different road types and speeds.

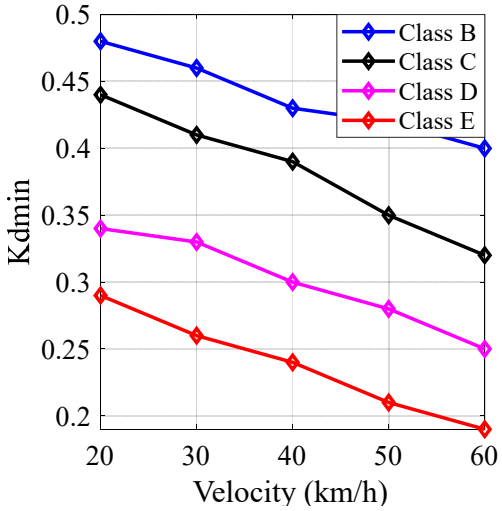


Figure 12. K_{dmin} varies across different road types and speeds.

Table 2. Results of surveying K_{dmax} and K_{dmin} under different speed and road surface conditions.

Speed	Road Class	B		C		D		E	
	Value	K_{dmax}	K_{dmin}	K_{dmax}	K_{dmin}	K_{dmax}	K_{dmin}	K_{dmax}	K_{dmin}
	20	1.12	0.48	1.23	0.44	1.43	0.34	1.64	0.29
	30	1.16	0.46	1.25	0.41	1.49	0.33	1.71	0.26
	40	1.23	0.43	1.31	0.39	1.58	0.30	1.82	0.24
	50	1.29	0.42	1.39	0.35	1.65	0.28	1.94	0.21
	60	1.34	0.40	1.43	0.32	1.78	0.25	2.03	0.19

The effect of road surface roughness outweighs speed: At the same speed range (v = 60 km/h), when road surface roughness changes from grade B to grade E, K_{dmax} increases from 1.34 to 2.03 (a 51.5% increase). Meanwhile, on the same grade E road surface, increasing speed from 20 km/h to 60 km/h only increases K_{dmax} from 1.64 to 2.03 (a 23.8% increase).

The degree of traction loss: A K_{dmin} threshold of 0.50 is defined as the warning point at which the safety of movement begins to decrease, and $K_{dmin} = 0$ is the limit of complete wheel separation from the road surface. On road types B and C, the K_{dmin} value ranges from 0.48 to 0.32, ensuring the vehicle maintains stable longitudinal and lateral force transmission. However, on road types D and E, the K_{dmin} decreases significantly. Even at 20 km/h, the K_{dmin} drops to 0.34 (road D) and 0.29 (road E). Under ISO 8608 road class E at a vehicle speed of 60 km/h, the minimum dynamic load coefficient (K_{dmin}) decreases to 0.19, indicating a substantial reduction in the tire–road contact force. Although this value remains above the complete wheel separation threshold ($K_{dmin} = 0$), it suggests an increased risk of intermittent loss of tire–road contact under severe operating conditions.

4. The Effect of Rear Suspension Stiffness

In this study, only the rear suspension stiffness coefficients (C_{21} and C_{22}) were varied, while the front suspension parameters were maintained at their baseline values. This approach was adopted to isolate the influence of rear suspension stiffness on the vertical dynamic loads acting on the drive axle housing. The effect of rear suspension stiffness on the dynamic loading on the axle housing was studied, with C_{21} and C_{22} varying from 0.5 to 1.5 times the initial value under varied speed and road-class conditions. The acquired data were used to analyze variations in K_{dmax} and K_{dmin}, thereby determining the extent of suspension stiffness's influence on dynamic loads and the bearing capacity of the axle housing.

As shown in Figures 13–16, the vertical dynamic load F_{z2} on the rear wheel increases with changes in road surface conditions from type B to type E. On road types B and C, changes in suspension stiffness from 0.5*C to 1.5*C altered the amplitude of load oscillation, but the difference between cases was not significant. With the deterioration of the road surface (types D and E), dynamic loads increase sharply, and the differences in stiffness are more pronounced. Specifically, suspension systems with a stiffness of 1.5*C tend to increase the amplitude of dynamic load, while a stiffness of 0.5*C helps reduce the degree of load oscillation. The results show that the road surface quality and suspension stiffness significantly influence the dynamic load on the rear axle. These observations are further supported by the quantitative results presented in Table 3, where the maximum and

minimum dynamic load coefficients (K_{dmax} and K_{dmin}) are used to characterize the effects of road roughness, vehicle speed, and suspension stiffness on the dynamic wheel load response.

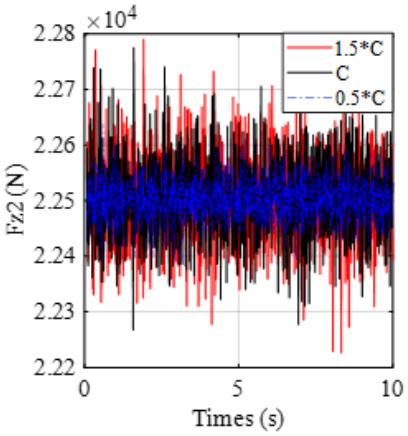


Figure 13. F_{z2}, 60 km/h when changing suspension stiffness on class B.

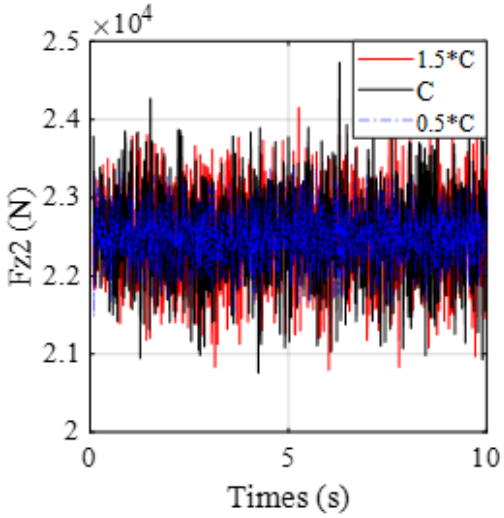


Figure 14. F_{z2}, 60 km/h when changing suspension stiffness on class C.

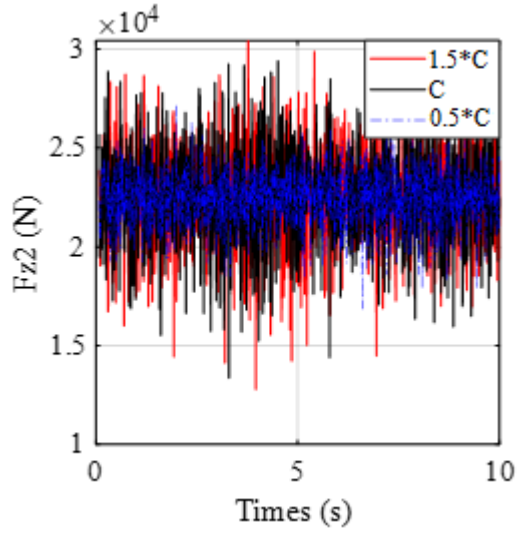


Figure 15. F_{z2}, 60 km/h when changing suspension stiffness on class D.

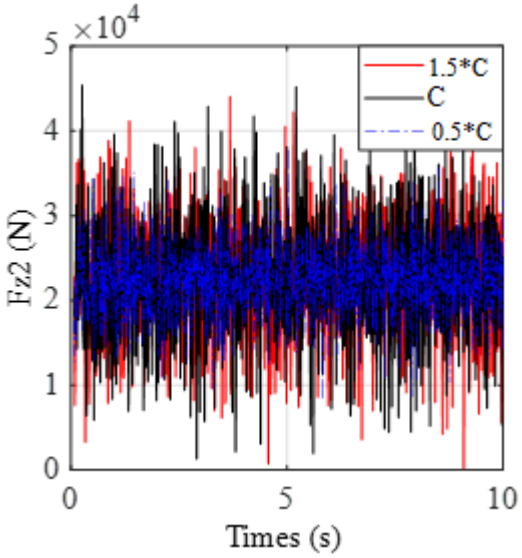


Figure 16. F_{z2}, 60 km/h when changing suspension stiffness on class E.

Table 3. The influence of vehicle speed and suspension stiffness on dynamic load coefficients K_{dmax} and K_{dmin} on different road types.

Speed	Evaluation Criteria	Road	Suspension Stiffness (*C)					
			0.5*C	0.7*C	0.9*C	1.1*C	1.3*C	1.5*C
20 km/h	K_{dmax}	B	1.02	1.05	1.11	1.2	1.23	1.28
		C	1.11	1.18	1.22	1.26	1.31	1.35
		D	1.23	1.31	1.38	1.45	1.49	1.55
		E	1.46	1.53	1.62	1.73	1.79	1.86
	K_{dmin}	B	0.54	0.51	0.49	0.46	0.44	0.42
		C	0.48	0.46	0.45	0.43	0.4	0.37
		D	0.38	0.36	0.35	0.33	0.31	0.3
		E	0.33	0.31	0.3	0.28	0.27	0.25
30 km/h	K_{dmax}	B	1.04	1.07	1.14	1.24	1.3	1.34
		C	1.14	1.2	1.23	1.31	1.36	1.39
		D	1.38	1.46	1.56	1.59	1.65	1.72
		E	1.48	1.56	1.65	1.77	1.84	1.9
	K_{dmin}	B	0.52	0.5	0.48	0.45	0.43	0.4
		C	0.47	0.45	0.43	0.4	0.38	0.36
		D	0.37	0.35	0.34	0.32	0.3	0.28
		E	0.3	0.28	0.27	0.25	0.24	0.22
40 km/h	K_{dmax}	B	1.14	1.16	1.21	1.3	1.35	1.39
		C	1.21	1.24	1.29	1.38	1.42	1.47
		D	1.53	1.61	1.66	1.73	1.79	1.85
		E	1.58	1.67	1.77	1.89	1.96	2.08
	K_{dmin}	B	0.49	0.47	0.44	0.42	0.4	0.37
		C	0.44	0.42	0.4	0.38	0.36	0.34
		D	0.33	0.31	0.3	0.29	0.27	0.25
		E	0.25	0.23	0.23	0.23	0.22	0.21
50 km/h	K_{dmax}	B	1.18	1.21	1.26	1.34	1.38	1.42
		C	1.27	1.31	1.37	1.45	1.49	1.53
		D	1.62	1.7	1.78	1.83	1.88	1.97
		E	1.72	1.81	1.92	2.06	2.12	2.25
	K_{dmin}	B	0.43	0.41	0.41	0.41	0.39	0.37
		C	0.35	0.33	0.31	0.34	0.32	0.31
		D	0.29	0.27	0.26	0.27	0.26	0.24
		E	0.22	0.21	0.2	0.2	0.19	0.18
60 km/h	K_{dmax}	B	1.26	1.3	1.32	1.38	1.45	1.48
		C	1.35	1.39	1.41	1.46	1.53	1.57
		D	1.68	1.75	1.82	1.89	1.94	2.01
		E	1.82	1.91	1.99	2.11	2.23	2.3
	K_{dmin}	B	0.41	0.4	0.4	0.39	0.37	0.35
		C	0.36	0.34	0.33	0.31	0.3	0.28
		D	0.26	0.25	0.25	0.24	0.23	0.22
		E	0.22	0.21	0.2	0.19	0.18	0.17

As suspension stiffness increases from 0.5*C to 1.5*C, the K_{dmax} value increases continuously. An overly stiff suspension reduces vibration absorption, leading to greater wheel force on the road surface. Conversely, K_{dmin}

generally tends to decrease as suspension stiffness increases, although slight increases or unchanged values are observed. As vehicle speed increases from 20 km/h to 60 km/h, K_{dmax} increases significantly, and K_{dmin} decreases significantly. Higher vehicle speeds generate stronger vibrations due to increased frequency of road surface impacts. The worse the road surface quality (from B to E), the greater the road surface undulation amplitude, leading to K_{dmax} increasing sharply (on type E roads, K_{dmax} exceeds 2.0 at high speeds) and K_{dmin} decreasing significantly (below 0.20).

Increasing rear suspension stiffness leads to higher K_{dmax} and lower K_{dmin}, particularly on rough roads, indicating greater dynamic wheel loads and reduced tire–road contact forces. Conversely, excessively low stiffness may increase suspension deflection and affect vehicle stability. Therefore, a stiffness range of 0.7*C–0.9*C is suggested as a reasonable compromise between limiting dynamic loads and maintaining tire–road contact under the investigated operating conditions.

Figure 17 illustrates the K_{dmax} value for a type B road at different speeds and suspension stiffnesses. The K_{dmax} value varies slightly from 1.02 (at 20 km/h, stiffness 0.5*C) to 1.48 (at 60 km/h, stiffness 1.5*C). Because Type B roads are of good quality and have a relatively smooth surface, the dynamic load acting on the car is relatively small and gentle. Figure 18 illustrates the K_{dmin} values for road class B under different vehicle speeds and suspension stiffnesses. K_{dmin} ranges from 0.35 to 0.54, with the minimum value of 0.35 observed at 60 km/h and a suspension stiffness of 1.5*C. These results indicate that the minimum tire–road contact force decreases as vehicle speed and suspension stiffness increase.

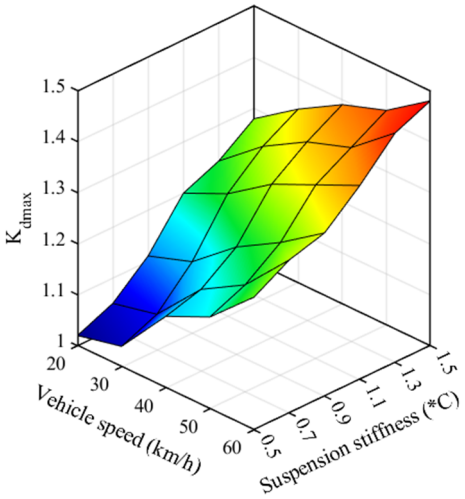


Figure 17. K_{dmax}, on class B.

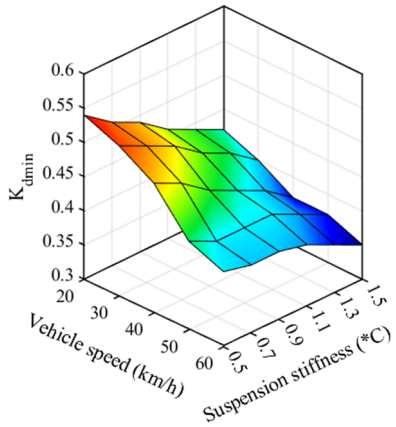


Figure 18. K_{dmin}, on class B.

Figure 19 illustrates the K_{dmax} value for a type C road at different speeds and suspension stiffnesses. The K_{dmax} value ranges from 1.11 to 1.57, and compared to road class B, K_{dmax} on road class C increases slightly under all speed and suspension stiffness conditions. Figure 20 illustrates the K_{dmin} value on a type C road with different speeds and suspension stiffness, K_{dmin} varies from 0.28 to 0.48. At 60 km/h and a high stiffness of 1.5*C, K_{dmin} decreases to 0.28, indicating reduced traction between the wheels and the road surface.

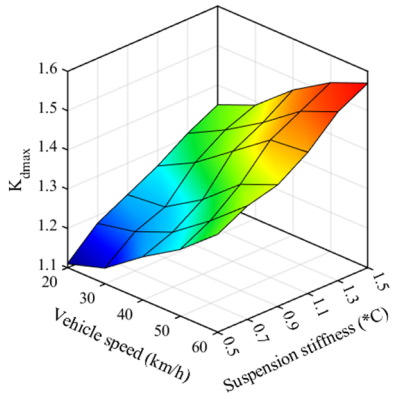


Figure 19. K_{dmax}, on class C.

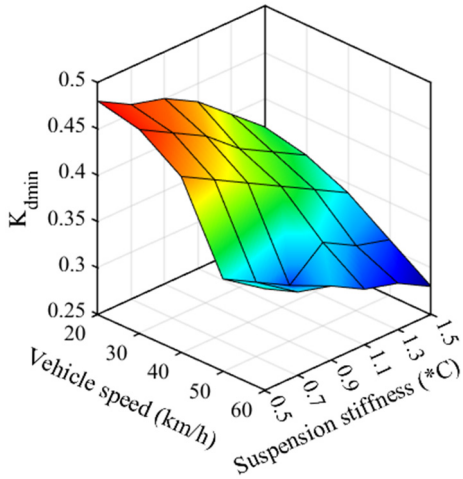


Figure 20. K_{dmin}, on class C.

Figure 21 shows the K_{dmax} value for a type D road at different speeds and suspension stiffnesses. The dynamic range of K_{dmax} increases significantly, fluctuating from 1.23 to 1.95. At 50–60 km/h and high suspension stiffness (1.1*C to 1.5*C), K_{dmax} is always greater than 1.40, leading to large dynamic loads on the road structure and the vehicle body. Figure 22 shows the K_{dmin} values for road class D at different vehicle speeds and suspension stiffnesses. K_{dmin} decreases significantly from 0.38 at 20 km/h and a suspension stiffness of 0.5*C to 0.22 at 60 km/h and a suspension stiffness of 1.5*C, indicating a substantial reduction in the minimum tire–road contact force.

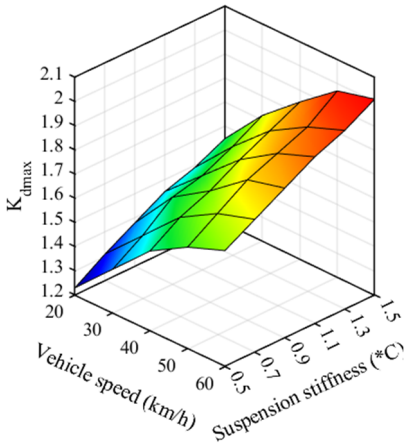


Figure 21. K_{dmax}, on class D.

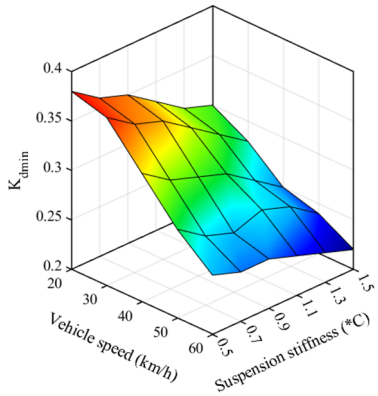


Figure 22. K_{dmin}, on class D.

Figure 23 shows the K_{dmax} value for a type E road at varying speeds and suspension stiffness. K_{dmax} is between 1.46 and 2.30, and this is the worst-case situation. At 60 km/h and a suspension stiffness of 1.5*C, K_{dmax} reaches 2.30, corresponding to a maximum vertical load 130% higher than the static load, which may increase structural stress fluctuations and fatigue-related risks. Figure 24 shows the K_{dmin} value for a type E road at varying speeds and suspension stiffnesses. K_{dmin} reduces to very low values, from 0.17 to 0.33, especially at 60 km/h, where it drops to 0.17–0.22. When the K_{dmin} value is near 0, there is a high chance the wheels will lift off the road surface, leading to loss of steering control and unsafe braking.

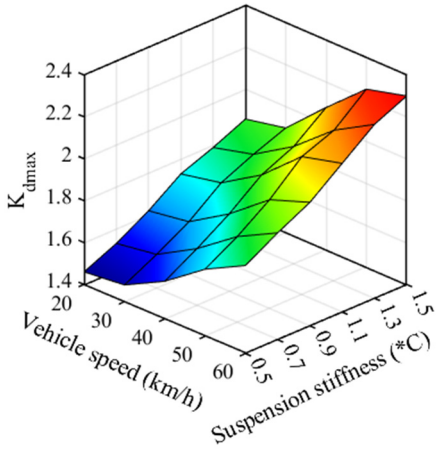


Figure 23. K_{dmax}, on class E.

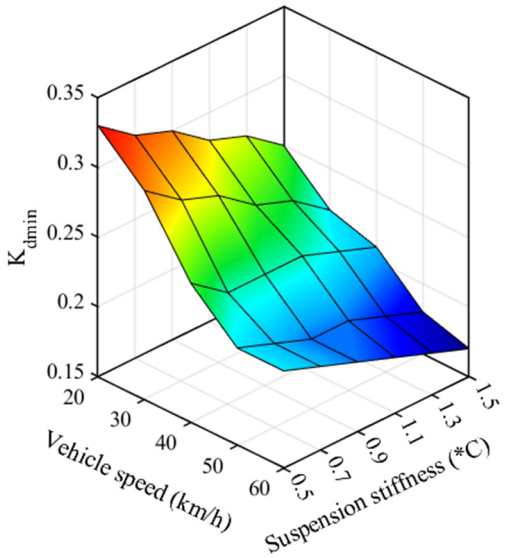


Figure 24. K_{dmin}, on class E.

5. Experimental Validation of the Vehicle Dynamic Model

To evaluate the reliability of the proposed full-vehicle dynamic model, additional simulations were conducted under road-bump excitation. Due to limitations in the available experimental facilities and measurement equipment, direct measurement of the dynamic vertical loads acting on the rear drive axle housing could not be performed. Therefore, the experimental validation was conducted using the vertical acceleration of the vehicle body as an alternative response parameter. The simulated body accelerations were compared with experimental measurements obtained under corresponding vehicle speeds, loading conditions, and road-bump excitations. This comparison provides an indirect assessment of the reliability of the proposed full-vehicle dynamic model in reproducing the vehicle's vertical dynamic response. A three-axis acceleration sensor (TAG-32150M7-25-VR-EGA) was used to measure vehicle body accelerations along the X, Y, and Z directions. The sensor was securely mounted on the vehicle body above the rear drive axle (Figure 25) and connected to a Kistler DAS-3 Data Acquisition System for signal acquisition and recording (Figure 26). The maximum absolute values of the measured vertical acceleration (Z-axis) were determined and compared with the corresponding numerical simulation results to evaluate the reliability of the proposed vehicle dynamic model.



Figure 25. Acceleration sensor (TAG-32150M7-25-VR-EGA) and location for installing the accelerometer on the vehicle.

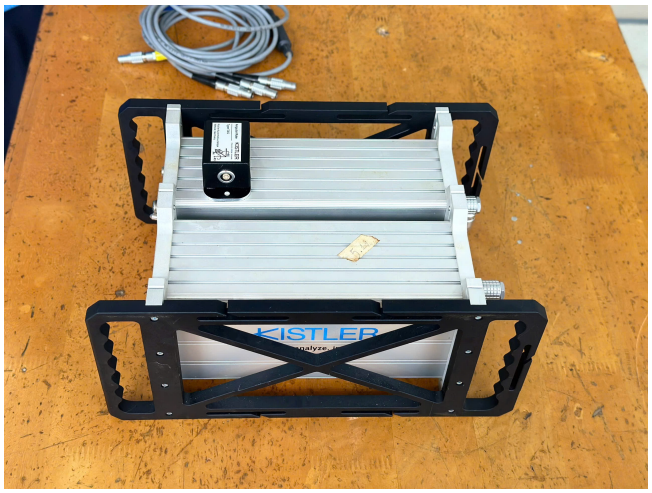


Figure 26. Kistler DAS-3 Data Acquisition System.

The experimental tests were conducted on a 1.25-ton light truck travelling over a road bump at different vehicle speeds. The road bump had a height of 45 mm and a longitudinal length of 345 mm (Figure 27). To reproduce the experimental conditions, the road excitation was represented by a half-cosine profile in the numerical model. The vehicle parameters, loading conditions, and suspension characteristics were maintained consistently between the numerical simulations and experimental tests.



Figure 27. Experimental road section.

The experimental tests were conducted at three vehicle speeds of 20, 30, and 40 km/h under the same road-bump excitation conditions. For each operating condition, the maximum absolute vertical body acceleration was determined from the experimental measurements and compared with the corresponding numerical simulation results. The results are summarized in Table 4, Figures 28 and 29.

Table 4. Comparison of maximum absolute vertical body accelerations between numerical simulations and experimental measurements at different vehicle speeds.

Vehicle Speed (km/h)	Simulation (m/s^2)	Experiment (m/s^2)	Error (%)
20 km/h	6.31	6.60	4.39
30 km/h	9.32	9.84	5.28
40 km/h	14.41	15.47	6.85

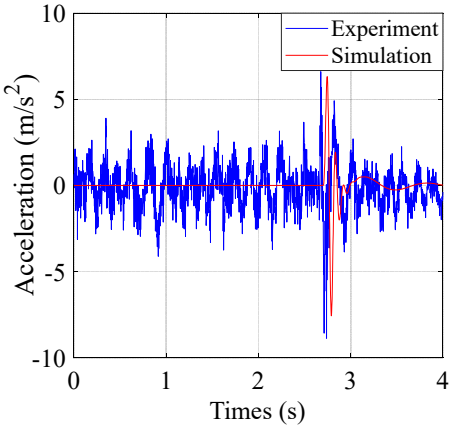


Figure 28. Vertical acceleration, velocity 20 km/h.

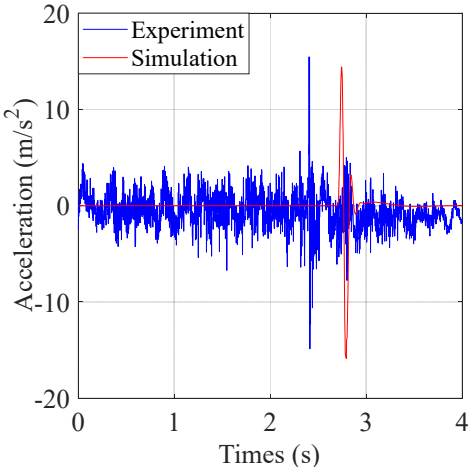


Figure 29. Vertical acceleration, velocity 40 km/h.

As shown in Table 4 and Figure 30, the simulation results agree well with the experimental measurements at all three vehicle speeds. The relative errors are 4.39%, 5.28%, and 6.85% at 20, 30, and 40 km/h, respectively. Although the simulated maximum accelerations are slightly lower than the experimental values, the discrepancies remain below 7%. This agreement supports the reliability of the proposed vehicle dynamic model in predicting vertical acceleration under the investigated operating conditions.

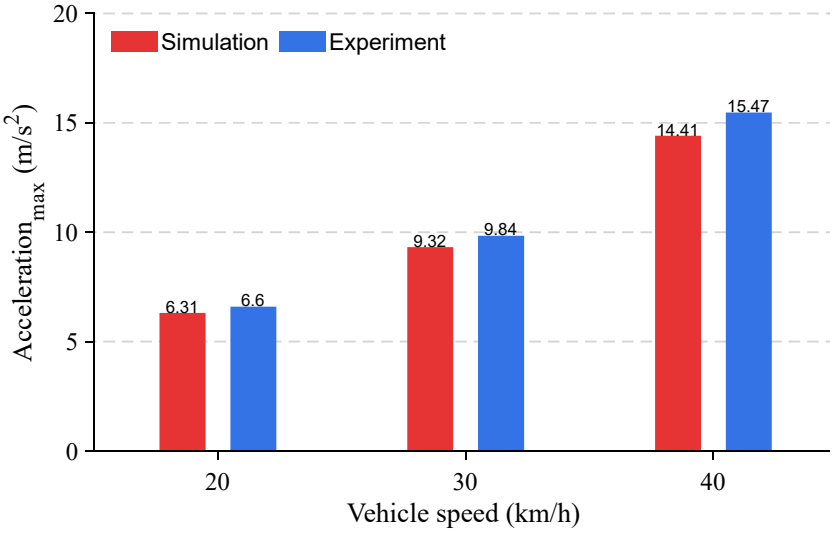


Figure 30. Comparison of maximum absolute vertical body acceleration between numerical simulations and experimental measurements.

6. Conclusions

In this work, a full-vehicle vibration model was developed to examine the combined effects of road surface roughness, vehicle speed, and rear suspension stiffness on the dynamic load acting on the drive axle housing of a 1.25-ton light truck. The simulation results lead to the following main conclusions:

The main factors impacting the dynamic loading of the axle housing are the roughness of the road surface. For the same speed of 60 km/h, the value of K_{dmax} increases from 1.34 to 2.03 (51.5%), while the value of K_{dmin} reduces from 0.40 to 0.19 (52.5%) when the road class changes from B to E. Bad road surfaces significantly increase the load on the axle housing.

The dynamic load transferred to the rear axle depends on the suspension system's stiffness. Increasing stiffness from 0.5*C to 1.5*C increases K_{dmax} across all road types and decreases K_{dmin}. For road class E at 60 km/h, K_{dmax} rises from 1.82 to 2.30 (26.4%). Simultaneously, K_{dmin} decreases from 0.22 to 0.17 (a 22.7% decrease), indicating that a too-stiff suspension reduces vibration absorption and increases the dynamic forces imparted to the axle structure.

For roads of class E, the velocity increases from 20 to 60 km/h, and K_{dmax} increases from 1.65 to 2.02 (an increase of 22.4%). At the same time, K_{dmin} is reduced from 0.29 to 0.19, which increases the probability of motion instability and reduces the wheel's ability to transmit power.

The most critical operating condition occurs on road class E at 60 km/h with a suspension stiffness of 1.5*C, where K_{dmax} reaches 2.30, corresponding to a maximum vertical load 130% higher than the static load. Meanwhile, K_{dmin} decreases to 0.17, indicating a substantial reduction in the tire–road contact force to 17% of its static value. Although complete wheel lift-off is not predicted under this condition, the significantly reduced normal force may adversely affect tire–road adhesion and vehicle stability.

Based on the numerical results, suspension stiffness values ranging from 0.7*C to 0.9*C may provide a favorable compromise between dynamic loading and tire–road contact under rough road conditions. This reduction in dynamic load fluctuations may potentially benefit axle housing durability. It should be noted that the present study does not systematically investigate the effects of damping coefficient, tire stiffness, or vehicle payload. Therefore, the recommended suspension stiffness range of 0.7*C–0.9*C is limited to the investigated vehicle configuration and operating conditions.

The present study is limited by the assumptions of linear suspension and tire characteristics and the use of a single vehicle configuration. Although experimental comparisons showed good agreement in vertical body acceleration, direct validation of dynamic axle loads remains necessary. Future research will incorporate nonlinear

suspension characteristics, experimental measurements of axle loads, and structural stress and fatigue-life assessments of the drive axle housing under representative operating conditions.

Author Contributions: L.V.V.: Conceptualization, supervision, project administration. N.T.D.: Methodology, formal analysis. T.N.L.: Software, simulation. T.T.N.T.: Data curation, visualization, writing—original draft preparation, writing—review and editing. D.H.D.: Investigation, validation, literature review. All authors have read and agreed to the published version of the manuscript.

Funding: This research received no external funding.

Institutional Review Board Statement: Not applicable.

Informed Consent Statement: Not applicable.

Data Availability Statement: The data supporting the findings of this study are available from the corresponding author upon reasonable request. The MATLAB/Simulink models and simulation parameters used in this study can also be provided for research purposes.

Acknowledgments: The authors would like to thank the Faculty of Mechanical and Power Engineering, Vinh Long University of Technology Education, for supporting this research.

Conflicts of Interest: The authors declare no conflict of interest.

Use of AI and AI-Assisted Technologies: During the preparation of this manuscript, the authors used ChatGPT (OpenAI) to improve English language, grammar, and manuscript readability. After using this tool, the authors carefully reviewed and edited the content and take full responsibility for the content of the published article.

References

1. Luong, V.V.; Cao, H.P.; Nguyen, T.T. Effect of Suspension System Stiffness on Dynamic Load Action Chassis Multi-purpose Forest Fire Fighting Vehicle. *Int. J. Eng.* **2022**, *35*, 1571–1578. https://doi.org/10.5829/ije.2022.35.08b.13.
2. Luong, V.V.; Nguyen, T.T. Effect of velocity and road quality to the dynamic load acting on the rear axle housing multifunction forest firefighting automotive. *Int. J. Interact. Des. Manuf.* **2025**, *19*, 2853–2863. https://doi.org/10.1007/s12008-024-01893-0.
3. Luong, V.V.; Nguyen, T.T.; Van, N.T.; Trai, M.P. Optimizing the Structure of the Axle Housing Multi-purpose Forest Fire Fighting Vehicle by Finite Element Method. In Proceedings of the 3rd Annual International Conference on Material, Machines and Methods for Sustainable Development (MMMS2022), Can Tho, Vietnam, 10–13 November 2022; Springer: Cham, Switzerland, 2023; pp. 277–284
4. Faris, W.F.; Ihsan, S.I.; Ahmadian, M. A comparative ride performance and dynamic analysis of passive and semi-active suspension systems based on different vehicle models. *Int. J. Veh. Noise Vib.* **2009**, *5*, 116–140. https://doi.org/10.1504/ijvnv.2009.029195.
5. Munawwarah, S.; Yakub, F. Control analysis of vehicle ride comfort through integrated control devices on the quarter and half car active suspension systems. *Proc. Inst. Mech. Eng. Part D J. Automob. Eng.* **2020**, *235*, 1256–1268. https://doi.org/10.1177/0954407020968300.
6. Abramov, S.; Mannan, S.; Durieux, O. Semi-active suspension system simulation using Simulink. *Int. J. Eng. Syst. Model. Simul.* **2009**, *1*, 101–114. https://doi.org/10.1504/ijesms.2009.027573.
7. Nhu, A.N.; Le, N.; Li, S.; Truong, T.D.V. Physics-Guided Reinforcement Learning System for Realistic Vehicle Active Suspension Control. In Proceedings of the International Conference on Machine Learning and Applications (ICMLA), Jacksonville, FL, USA, 15–17 December 2023; pp. 422–429. https://doi.org/10.1109/icmla58977.2023.00065.
8. Mo, S.; Chen, K.; Zhang, Y.; Zhou, Y.; Lyu, L.; Yao, B.; Zhang, W. Research on rigid-flexible coupling nonlinear dynamics of light commercial vehicle considering frame flexibility. *Int. J. Non-Linear Mech.* **2025**, *170*, 104949. https://doi.org/10.1016/j.ijnonlinmec.2024.104949.
9. Zheng, B.; Fu, S.; Lei, J. Topology Optimization and Multiobjective Optimization for Drive Axle Housing of a Rear Axle Drive Truck. *Materials* **2022**, *15*, 5268. https://doi.org/10.3390/ma15155268.
10. Shao, Y.; Liu, J.; Mechefske, C.K. Drive axle housing failure analysis of a mining dump truck based on the load spectrum. *Eng. Fail. Anal.* **2011**, *18*, 1049–1057. https://doi.org/10.1016/j.engfailanal.2010.12.023.
11. Zhang, L.X.; Liu, S.; Mao, E.R.; Xie, B.; Meng, X. Dynamic Load of Agricultural Machinery Drive Axle Housing Based on Field Measured Road Roughness. *Adv. Mater. Res.* **2013**, *834–836*, 1295–1298. https://doi.org/10.4028/www.scientific.net/amr.834-836.1295.
12. Zhao, W.; Sun, M.; Wang, H.; Meng, Q.; Fan, Z. Vehicle Response Calculation Under the Action of Random Road Spectrum and Fatigue Life Prediction of the Drive Axle Housing. *Adv. Sci. Lett.* **2012**, *12*, 95–99. https://doi.org/10.1166/asl.2012.2825.
13. *ISO 8608:2016*; Mechanical Vibration—Road Surface Profiles-Reporting of Measured Data. International Organization for Standardization: Geneva, Switzerland, 2016.

14. Luong, V.V.; Nguyen, T.T. Application of Air Suspension System on Multi-purpose Forest Fire Fighting Vehicle for Reducing Dynamic Load. *J. Vib. Eng. Technol*. **2024**, *12*, 7219–7230. https://doi.org/10.1007/s42417-023-01069-2.
15. Luong, V.V.; Nguyen, T.T. Speed and road quality effects on dynamic load multi-purpose forest firefighting vehicles. *Arch. Appl. Mech.* **2024**, *94*, 3359–3376. https://doi.org/10.1007/s00419-024-02672-9.
16. Hua, C.; Zhao, Y.; Lu, Z.; Ouyang, H. Random vibration of vehicle with hysteretic nonlinear suspension under road roughness excitation. *Adv. Mech. Eng.* **2018**, *10*, 1687814017751222. https://doi.org/10.1177/1687814017751222.
17. Misaghi, S.; Tirado, C.; Nazarian, S.; Carrasco, C. Impact of pavement roughness and suspension systems on vehicle dynamic loads on flexible pavements. *Transp. Eng.* **2021**, *3*, 100045. https://doi.org/10.1016/j.treng.2021.100045.
18. Wei, H.; Lu, J.; Lu, H.; Shi, L.; Wu, B.; Jiang, P. Hopf bifurcation and energy transfer of automobile shimmy system with consideration of road roughness excitation. *Veh. Syst. Dyn.* **2022**, *60*, 454–469. https://doi.org/10.1080/00423114.2020.1821903.
19. Zhang, B.; Tan, C.A.; Dai, T. Ride comfort and energy dissipation of vehicle suspension system under non-stationary random road excitation. *J. Sound Vib.* **2021**, *511*, 116347. https://doi.org/10.1016/j.jsv.2021.116347.
20. Nazemi, S.; Masih-Tehrani, M.; Mollajafari, M. GA tuned H_∞ roll acceleration controller based on series active variable geometry suspension on rough roads. *Int. J. Veh. Perform.* **2022**, *8*, 166–187. https://doi.org/10.1504/ijvp.2022.122047.
21. Najafi, A.; Masih-Tehrani, M. Roll stability enhancement in a full dynamic ground-tour vehicle model based on series active variable-geometry suspension. *Int. J. Veh. Perform.* **2022**, *8*, 188–223. https://doi.org/10.1504/ijvp.2022.122050.
22. Satyanarayana, V.S.V.; Sateesh, B.; Rao, N.M. Parameters optimisation of vehicle suspension system for better ride comfort. *Int. J. Veh. Perform.* **2018**, *4*, 186–199. https://doi.org/10.1504/ijvp.2018.090956.
23. Deremetz, M.; Lenain, R.; Thuilot, B. Stiffness and damping real-time control algorithms for adjustable suspensions: A strategy to reduce dynamical effects on vehicles in off-road conditions. *IFAC-PapersOnLine* **2017**, *50*, 1958–1964. https://doi.org/10.1016/j.ifacol.2017.08.1565.
24. Wang, C.; Ouyang, J.; Cao, P.; Song, J.; Yu, S. Development and Validation of 3D Commercial Vehicle Multibody Dynamics Model to Assess Dynamic Load Coefficient. *J. Transp. Eng. Part B Pavements* **2024**, *150*, 04024028. https://doi.org/10.1061/jpeodx.pveng-1429.
25. Gheibollahi, H.; Masih-Tehrani, M.; Najafi, A. Improving ride comfort approach by fuzzy and genetic-based PID controller in active seat suspension. *Int. J. Autom. Control.* **2024**, *18*, 184–213. https://doi.org/10.1504/ijaac.2024.137072.
26. Luong, V.V.; Nguyen, T.T. Dynamic Load Determination of a Multi-purpose Forest Fire Fighting Vehicle When Operating on Forestry Road. *J. Vib. Eng. Technol*. **2024**, *12*, 3507–3517. https://doi.org/10.1007/s42417-023-01061-w
27. Luong, V.V.; Nguyen, T.T. Determine the dynamic load acting on the chassis of multi-purpose forest fire fighting vehicle. *Proc. IOP Conf. Ser. Mater. Sci. Eng.* **2021**, *1173*, 012030. https://doi.org/10.1088/1757-899x/1173/1/012030.
28. Phan, T.T. Development of a Dynamic Model for Determining Dynamic Loads Acting on the Axle Housing of a 1.25-Ton Light Truck. Master's Thesis, Vinh Long University of Technology Education, Vĩnh Long, Vietnam, 2020.